



OPEN ACCESS

EDITED BY

Xiaohua Liu,
The Chinese University of Hong Kong, China

REVIEWED BY

Kangsen Li,
Shenzhen University, China
Zhang Canbin,
Shenzhen University, China

*CORRESPONDENCE

Oliver Huerta-Carranza,
✉ oliver@ciencias.unam.mx

RECEIVED 12 November 2025

REVISED 14 January 2026

ACCEPTED 23 January 2026

PUBLISHED 17 February 2026

CITATION

Santiago-Alvarado A, Granados-Agustin FS, Huerta-Carranza O, Cruz-Martinez VM, Alvarado-Martinez J and Avendaño-Alejo M (2026) Manufacturing of a toroidal mold for the production of polymeric lenses. *Adv. Opt. Technol.* 15:1745190. doi: 10.3389/aot.2026.1745190

COPYRIGHT

© 2026 Santiago-Alvarado, Granados-Agustin, Huerta-Carranza, Cruz-Martinez, Alvarado-Martinez and Avendaño-Alejo. This is an open-access article distributed under the terms of the [Creative Commons Attribution License \(CC BY\)](https://creativecommons.org/licenses/by/4.0/). The use, distribution or reproduction in other forums is permitted, provided the original author(s) and the copyright owner(s) are credited and that the original publication in this journal is cited, in accordance with accepted academic practice. No use, distribution or reproduction is permitted which does not comply with these terms.

Manufacturing of a toroidal mold for the production of polymeric lenses

Agustin Santiago-Alvarado¹, Fermín S. Granados-Agustin², Oliver Huerta-Carranza^{3*}, Víctor M. Cruz-Martínez¹, Jorge Alvarado-Martínez⁴ and Maximino Avendaño-Alejo⁴

¹División de Estudios de Posgrado, Universidad Tecnológica de la Mixteca, Huajuapán de León, Mexico, ²Coordinación de Óptica, Instituto Nacional de Astrofísica, Óptica y Electrónica, Tonanzintla-Puebla, Mexico, ³Departamento de Física, Facultad de Ciencias, Universidad Nacional Autónoma de México, Ciudad de México, Mexico, ⁴Instituto de Ciencias Aplicadas y Tecnología, Universidad Nacional Autónoma de México, Ciudad de México, Mexico

The manufacture of optical molds for generating optical components in continuous or batch production has become a great challenge as freeform components are increasingly required. New manufacturing techniques have emerged to meet these technological demands; however, freeform optics present previously unseen manufacturing challenges as traditional optical workshops are designed to produce components with spherical shapes. The mold technique is widely used for batch production, but the main challenge is mold manufacturing. Therefore, the manufacturing process of a toroidal 6061 aluminum optical mold is presented, using a CNC milling machine. To evaluate the finish of the toroidal surface, null screen tests and coordinate measurements were used as these methods allow changes in slopes across the entire surface to be measured in a single evaluation, which is not possible with other tests. The results obtained show that implementation is feasible at a reduced cost, with a Peak to-Valley (PV) error of 0.1806 mm and an Root Mean Square (RMS) of 0.0402 mm in the surface finish, which can be further improved by taking the polishing stage as a guide.

KEYWORDS

freeform optical, milling manufacture, optical molding, optical tests, toroidal mold

1 Introduction

Freeform surfaces are gaining popularity in new instruments because they enable the generation of desired concentrations, illumination, or images with fewer optical components, making instruments more compact, lightweight, and versatile than those based on traditional components (Rolland et al., 2021; Chen et al., 2012; Ding et al., 2008; Sha et al., 2021; Kumar et al., 2022). This has been made possible by the use of recent manufacturing techniques and the incorporation of polymeric optical materials as traditional techniques pose a great challenge due to inadequate infrastructure for producing them (Li et al., 2018; Brenner et al., 1993; Mali et al., 2021; Ottevaere et al., 2004; Roeder et al., 2019; Moskaleva et al., 2021; He et al., 2022).

The existing techniques for fabricating freeform surfaces include the following: precision glass molding, wet or dry etching photolithography, micro-drilling, hot embossing, laser machining, powder blasting, injection and compression molding, and electrochemical etching; although these techniques allow mass production, they present

challenges in the dissolution of the material in all directions, leading to imperfections in the components, long manufacturing times and die replacement, surface scaling, or poor adhesion of the particles subjected to the control of the engraved profile (Li et al., 2018; Mali et al., 2021; Moskaleva et al., 2021; Peixoto et al., 2022; Lu and Khim, 2001; Liu et al., 2019; Santiago-Alvarado et al., 2023; Asgar et al., 2021; Zhang and Liu, 2017; Gurganus et al., 2019; Gates et al., 2005; Zhou et al., 2021; Michaeli et al., 2009; Li et al., 2021; Moon et al., 2003; Loaldi et al., 2018; Huang, 2008; Mayer, 2007; Spina et al., 2012). Other techniques, such as grinding, ultra-precision diamond turning, micro-milling, local grayscale oxidation, direct laser writing, laser catapulting (Li et al., 2018; Gates et al., 2005; Li et al., 2021; Moon et al., 2003), and scanning beam lithography (e.g., electron beam, focused ion-beam, and particle-beam lithography) (Ottevaere et al., 2004; Roeder et al., 2019; Gates et al., 2005), still present challenges for mass production. Some of these manufacturing processes may require complicated setups, where optimal processing parameters must be found to avoid altering the desired optical parameters, such as profiles or the refractive index distribution, to prevent the generation of inhomogeneous index distribution, birefringence, or thermal residual stress due to shrinkage (Peixoto et al., 2022). Moreover, many of them are suitable only for micro- and nano-surfaces. For example, the electric discharge machining technique can produce components with a surface roughness less than 0.1 μm ; however, it has the disadvantage that the workpieces must be conductive, so it cannot be applied to all types of materials (Roeder et al., 2019).

Meanwhile, the e-beam writing technique, although achieving a roughness of less than 0.2 μm , only works over small areas due to the long processing time, making it desirable for manufacturing microstructures (Roeder et al., 2019).

For these reasons, injection-compression molding is widely used as it allows multiple optical elements to be manufactured using the same mold in a short period once the optimal molding parameters have been determined through the trial-and-error method. The greatest challenge with this technique lies in mold manufacturing, considering the mold material, its size and shape, and the number of components to be produced, while also requiring a high-quality surface finish (Asgar et al., 2021; Zhou et al., 2021). The techniques commonly used to manufacture molds include photolithography, micromachining, electroforming (EDM), pyrolysis, wet and dry etching, laser-assisted etching, diamond cutting ultra-precision, milling, vibration cutting and grinding, conventional laser ablation (Asgar et al., 2021; Gates et al., 2005; Zhou et al., 2021; Pelin et al., 2024; Li et al., 2017; Fang FZ. et al., 2013; Singh et al., 2021), micro-compression with polymer powder (Moon et al., 2003), stereolithography, and selective laser sintering (Roeder et al., 2019; Atwood et al., 1998). Alternative methods also include chemical and plasma etching, metal 3D printing, fused filament fabrication, selective laser sintering, and reactive ion etching (RIE) (Li et al., 2018; Roeder et al., 2019; Pelin et al., 2024). Turning, ion-beam engraving, hybrid techniques, photothermal expansion, CO₂ laser irradiation, photoresist reflow (Gates et al., 2005; Mayer, 2007; Chen et al., 2014), laser beam shaping, photopolymerization (Ottevaere et al., 2006), microjet printing (Ottevaere et al., 2006), electron-beam lithography (Li et al., 2018; Ottevaere et al., 2004; Roeder et al., 2019; Lee and Scherer, 2001), and patterned SU-8-

layer photolithography processes (Asgar et al., 2021; Yu et al., 2009). Other processes that are less widely used or have recently emerged are described in the literature (Li et al., 2018; Roeder et al., 2019; Gates et al., 2005; Spina et al., 2012; Davis et al., 2009). However, these require modern, sophisticated equipment that is expensive, has restricted access, and was primarily developed for producing micro- and nano-molds in polymeric materials. In addition, tests are required to evaluate the mold's parameters and verify its quality (Ottevaere et al., 2004; Peixoto et al., 2022; Lu and Khim, 2001; Liu et al., 2019; Santiago-Alvarado et al., 2023; Asgar et al., 2021; Gates et al., 2005; Huang, 2008; Mayer, 2007; Li et al., 2017; Fang FZ. et al., 2013; Singh et al., 2021; Davis et al., 2009; Zhong, 2020; Lasemi et al., 2010; Zhan et al., 2009). Verification is carried out by applying optical tests, among which the most used are interferometric tests, geometric tests, null screens, and coordinate measurement (Santiago-Alvarado et al., 2023; Huerta-Carranza et al., 2021).

In this study, the design and traditional milling combined with the polishing stage were selected to manufacture the toroidal insert mold because this approach is inexpensive, easily accessible and implementable, and does not require state-of-the-art technology (Li et al., 2018; Loaldi et al., 2018; Chen et al., 2014). Once the mold has been manufactured, the quality evaluation of the mold finish is carried out; as the changes in surface slopes are large, null screen tests and measurement coordinate tests are implemented.

These tests can evaluate convex surfaces with $f/\# < 1$ and freeform at low cost; they do not require additional elements, such as holograms or reference surfaces, making them favorable for this type of evaluation as it only involves the design of the screen and its implementation in the desired arrangement.

The remainder of this study is structured as follows: freeform surfaces are described in Section 2. In Section 3, the optical materials used to produce molds are presented. Section 4 describes the methodology implemented. Section 5 deploys the results, analysis, and discussions. Finally, the conclusions and references are provided in Sections 6, 7, respectively.

2 Freeform surfaces

Freeform surfaces lack rotational or linear symmetry, unlike traditional surfaces such as spherical or aspherical surfaces. They are known as non-axis rotational invariance surfaces, also referred to as axially unbalanced surfaces (Rolland et al., 2021; Fang F. et al., 2013). These surfaces are designed to have more precise light control and are opening new application possibilities. Freeform surfaces have been applied in augmented and virtual reality, automotive lighting, imaging systems, and lighting and concentration systems, among other applications (Kumar et al., 2022).

Freeform optical surfaces are a powerful tool in modern optical design, enabling innovative, high-performance solutions in advanced applications and mass production. Usually introduced in compact or high-precision optical systems, these surfaces have revolutionized traditional optical systems.

The mathematical description of freeform surfaces can be global or local; radial basis functions, splines, wavelets, hybrid stitched, 2-Q polynomials, X-Y polynomials, Zernike polynomials, and aspherical



FIGURE 1
Machining center used for manufacturing the mold.

surfaces with deformation terms have been reported (Kumar et al., 2022; Elgarisi et al., 2021; Gross et al., 2015; Ye et al., 2017; Broemel et al., 2017). In this study, the toroidal mold is mathematically described using Equation 1 (Santiago-Alvarado et al., 2025):

$$A_0 + A_1x + A_2y + A_3x^2 + A_4xy + A_5y^2 - z = 0, \quad (1)$$

with

$$A_3 = 1/2r_x \text{ and } A_5 = 1/2r_y,$$

where r_x and r_y are the curvature radii on axes x and y , respectively; A_i represents the coefficient; and x , y , and z are the Cartesian coordinates of the surface.

3 Materials

The materials used in mold manufacturing are diverse and depend on the type of application, the technique used for its manufacture, and the precision required in surface finishing, dimensions, durability, and the number of elements to generate. The chosen material must possess rigidity, thermal stability, low thermal expansion, wear resistance, hardness, and the capacity to produce a large number of elements.

The literature reports the use of metals, polymers, ceramics, wood, fiberglass, quartz, glass, and other materials (He et al., 2022; Liu et al., 2019; Santiago-Alvarado et al., 2023; Ottevaere et al., 2006; Visconti et al., 2013; Carrasco Morcillo, 2019). In particular, metals including stainless steel, aluminum, germanium, zinc sulfide, zinc selenide, metal alloys with copper, nickel, iron, electroless nickel-phosphorus, tungsten carbide, silicon carbide, and metaloglass, which are combinations of metal and glass, have also been used (Chen et al., 2012; Sha et al., 2021). Since the mold presented in this study must guarantee the generation of several elements and is exposed to the melting temperatures of the polymer used, it was considered to be made of Aluminum 6061, which meets these requirements.

Aluminum 6061 is a 6000-series hardened aluminum alloy containing magnesium and silicon. It is versatile, lightweight, easy to machine, recyclable, offers good weldability, and has high corrosion resistance. It has medium-to-high strength compared to that of some mild or low-carbon steels. It can be easily cut and molded, reducing production costs and allowing the creation of complex parts with high precision.

Its ease of processing makes it a cost-effective option for many industrial applications. Due to its excellent mechanical properties, it reduces machining time, extends the life of the cutters, and allows the production of complex-shaped parts. It has low density, is heat-treatable, has a melting point between 582 °C and 652 °C, and exhibits good thermal (167 W/m-K) and electrical conductivity (Bohórquez et al., 2010; Coppermetal, 2025).

In this work, a five-axis CNC vertical machining center (Challenger MM 430) with a table size of 90 cm × 43 cm ×

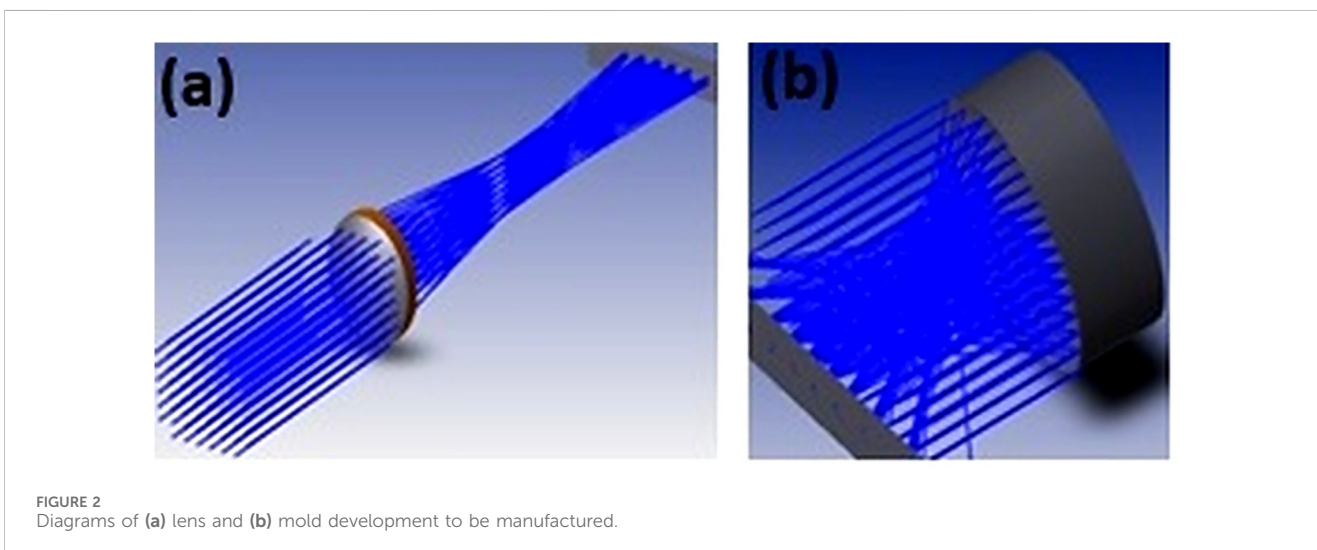
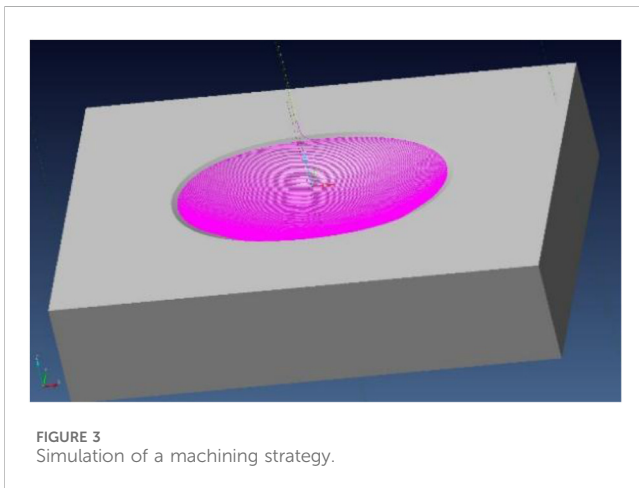


FIGURE 2
Diagrams of (a) lens and (b) mold development to be manufactured.

TABLE 1 Sample start of machining codes.

%Toroidal mold, MX--	N14 M8	N19 X0.84 Z3.252
N1 G90	N15 Z5.585	N20 X1.2 Z3.069
N2 T01 M06	N16 G1 Z4.295 F800	N21 X1.598 Z3.005
N3 G54	N17 X0.372 Z3.897	N22 X1.806 Y-2.884 Z2.999
N12 G0 X0.308 Y-2.901 S3500 M03	N18 X0.555 Z3.537	N23 X2.008 Y-2.831 Z2.992



40 cm and AT&O[®] solid carbide vertical cutting tools with X-FACTOR[®] coating was used. Figure 1 shows the milling machine.

4 Methodology for manufacturing and testing the mold

The process to manufacture the aluminum 6061 toroidal mold using a machining center CNC is as follows: 1) the design of the optical component and the required mold is performed using optical theory or design software, validating their performance; 2) the computer-aided design (CAD) and computer-aided manufacture (CAM) models of the mold are generated using finite element software (FES); 3) machining codes required are generated using a milling machine; 4) machining strategies and parameters should be chosen to reduce the machining footprints left by cutting tools (related to roughness); 5) a polishing stage is implemented to erase traces of the cutters when changing paths; and 6) optical testing stages are applied to verify the surface shape finish.

The process begins with the optical design of the lens, and from this, the mold is designed using FES (Ansys Zemax OpticStudio[®]). In this case, a toroidal convex-plane lens was designed, where the toroidal surface has radii $R_x = 23$ mm and $R_y = 64$ mm, with a major axis diameter of 32 mm in the Y-axis and a minor axis diameter of 20 mm in the X-axis, a marginal thickness of 6 mm, and a paraxial thickness of 2.28 mm; diagrams of the lens and mold designs are shown in Figure 2.

The profile of the mold surface was designed to produce convex toroidal surfaces with differing X and Y curvatures (more than double) to determine which methods can evaluate the entire surface without additional elements, for application human eye cornea

assessments. Because interferometric tests cannot measure large changes in the wavefront slope in a complete measurement, it is necessary to evaluate in parts or with additional elements.

After validating the mold design using design software, the resulting CAD file generated is used to create the machining code (see Table 1), from which the machining strategy and parameters are chosen to minimize processing time and reduce cutter marks on the mold surface. Simulations of the machining strategy allow assessment of the feasibility of the operations, as shown in Figures 3, 4.

The simulations indicate the type of operations that can be carried out during the roughing and finishing processes, depending on the type of surface to be generated. This also allows us to know the feed speed and cutting depth ranges, the cutter revolutions range, and the number of flutes to be used. The manufacturing technician selects the appropriate machining parameters from these options. The optimal selection of machining parameters can be determined through an experimental design, which yields the lowest surface roughness, as reported in the literature (Hazir et al., 2018).

Once the mold has been machined, a polishing stage is carried out to remove the machining marks left by the cutting tool on the workpiece. The polishing process implemented is similar to that of classical polishing. It begins with the use of fine-grained sandpaper numbers 1500 and 2000, for an average time of 20 min. Afterward, the surface is rinsed and polished with Terazit 2402 abrasive paste for 10 min using cotton pads, followed by polishing for an additional

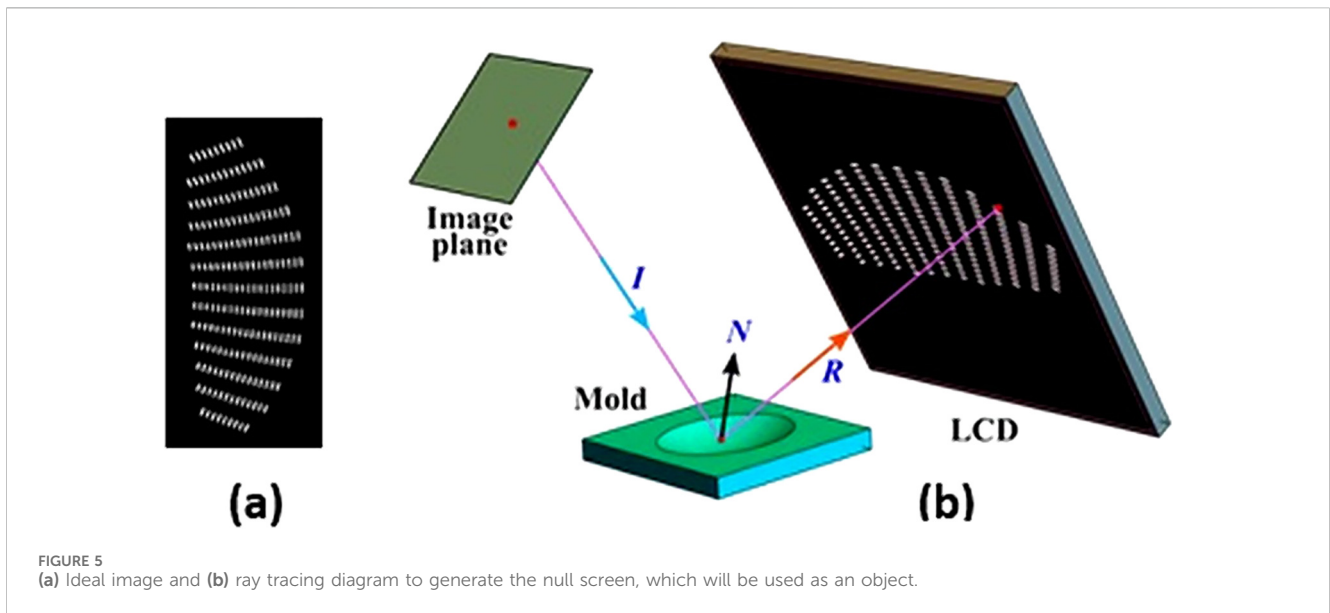


FIGURE 5
(a) Ideal image and (b) ray tracing diagram to generate the null screen, which will be used as an object.

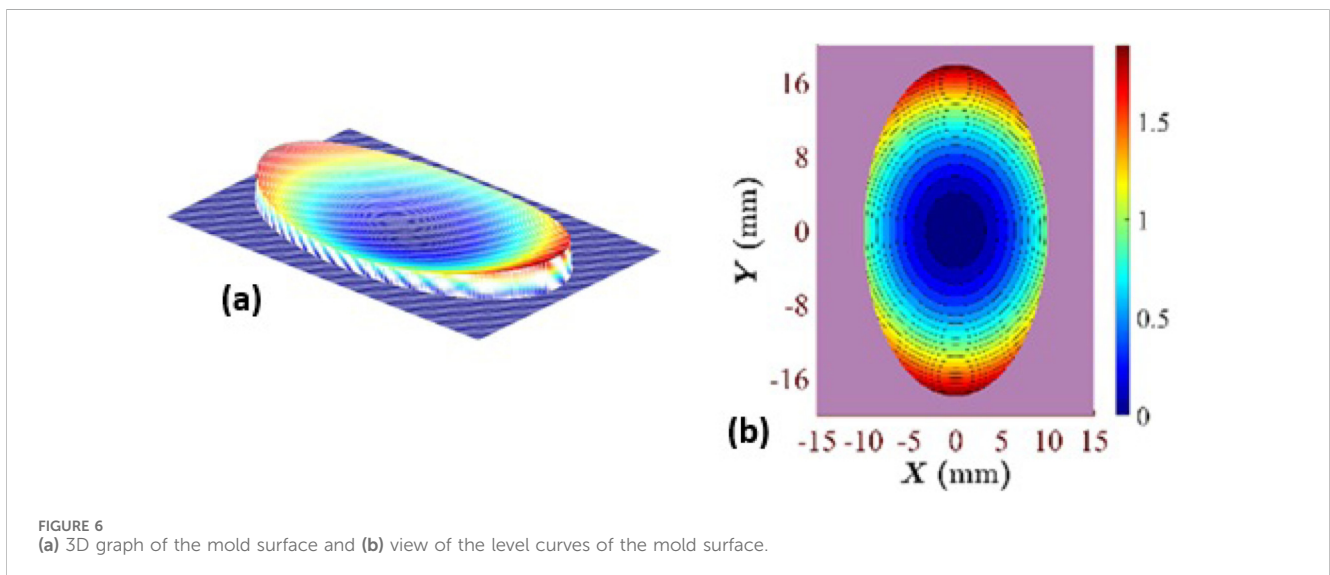


FIGURE 6
(a) 3D graph of the mold surface and (b) view of the level curves of the mold surface.

10 min with silicon-based polishing paste (1422 Austromex high-concentration diamond paste, 1 μm). In the process, a mototool is used; the surface is observed and qualitatively tested. Once finished, the surface is quantitatively evaluated.

Finally, the surface quality of the mold produced must be validated; for this purpose, two optical tests are implemented: the null screen test and the coordinate-measuring machine. These allow the measurement of surface profiles with rapid slope changes as conventional interferometry cannot quantify these phase changes without requiring additional elements.

In turn, the null screen test only requires designing the experimental setup and generating the null screen, and the coordinate measurement test needs to define the experimental arrangement to measure the mold profile using a position sensor. Both tests, after being applied, require processing the information to know the shape of the mold surface under test.

First, the application of the null screen test is described [a detailed description of the ray tracing and the mathematical theory used in the test is provided by Huerta-Carranza et al. (2021), Díaz-Urbe and Campos-García (2000), Aguirre-Aguirre et al. (2018), and Avendaño-Alejo et al. (2009)]. The test consists of the following: 1) designing an experimental arrangement to evaluate the surface of the mold; 2) choosing the shape of the image that the mold surface will form (ideal image); 3) calculating the shape of the null screen that will serve as the object; 4) performing the surface test by placing each element in the established position; 5) capturing the image produced by the mold surface using a CCD camera; and 6) processing the captured image by comparing it with the desired image. If the surface under test has the desired profile, the generated image will be identical to the ideal image; otherwise, the surface profile can be determined by quantifying the deviations in the image.

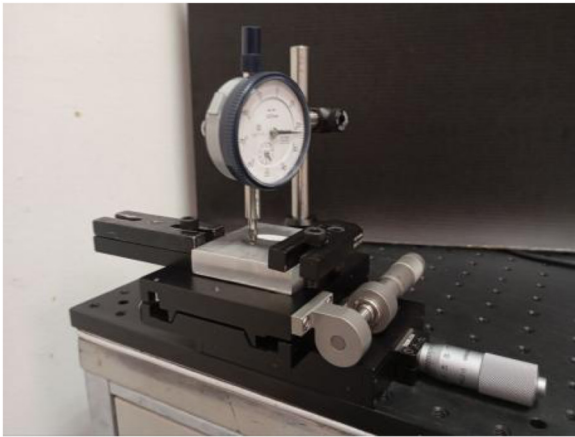


FIGURE 7
Experimental setup to test the workpiece by measuring coordinates.

The reference screen (null screen) is obtained by reverse ray tracing, considering the ideal shape of the mold surface. This suggests that the null screen is designed by performing a reverse ray path from the points that form the desired image (image plane) to the surface of the mold (ideal) to calculate the directions of the incident (I), reflected (R), and normal (N) rays and finally obtain the coordinates of the points where the rays intercept the plane of the object. When performing this process by sweeping the image plane, the object reference screen is constructed (see Figure 5). Once the null screen is generated, it is displayed on the liquid crystal screen (LCD) and projected onto the surface of the mold, forming its image (Santiago-Alvarado et al., 2023; Huerta-Carranza et al., 2021). When quantifying deviations, the shape of the mold surface is known.

To evaluate the toroidal mold surface, the setup shown in Figure 5 was implemented, where Figure 5a shows the null

screen image and Figure 5b shows the schematic diagram of the proof to be implemented.

The ideal surface of the mold is described using Equation 1, and toroidal parameters given at the beginning of Section 4 were taken for designing and applying a geometrical test based on the null screen method (Huerta-Carranza et al., 2025). The coefficients used are $A_0 = -2$ mm, $A_1 = 0$, $A_2 = 0$, $A_3 = 1/(2r_x)$, $A_4 = 0$, and $A_5 = 1/(2r_y)$, with $r_x = 23$ mm and $r_y = 64$ mm, as the reference center is 2 mm above the vertex of the toroidal face of the mold. Level curves of the mold were generated, as shown in Figure 6.

Once the null screen has been calculated, it is displayed on an LCD, and the implementation of the geometrical null test is carried out in the laboratory to generate the desired image (null image). An LCD was used to display the object pattern as it allows for the easy design of the null screen (Huerta-Carranza et al., 2025; Huerta-Carranza et al., 2024). In the experimental implementation, the following values are considered: pinhole position $h = (4.58$ mm, -78.068 mm, and 167.00 mm), focal length of the lens = 16 mm, and LCD center at $Q_0 = (-2.21$ mm, 32.80 mm, and 45.44 mm); the components of the unit vector normal to the plane of the LCD are $(-0.013, -0.745, \text{ and } -0.667)$, and the origin is located at the center of the surface. An EO-5023C 2/3" color CCD camera from Edmunds Optics was used for this purpose.

The object pattern or the null screen is displayed on an LCD with dimensions $L_x = 107.70$ mm, $L_y = 172.31$ mm, $P_x = 800$ pixels, and $P_y = 1,280$ pixels.

The image obtained (Figure 11b) is processed to determine the centroids of the bright spots. These points, along with the pinhole position, are used to calculate the directions of the incident rays $I = (I_x, I_y, I_z)$. The reflected rays $R = (R_x, R_y, R_z)$ are calculated using the intersection of the incident rays I with the design surface (see Equation 1) and the points of the object displayed on the LCD. Once both rays are known, the slopes to the surface under test can be calculated using Equation 2:

$$S_x = \frac{R_x - I_x}{R_z - I_z}; \quad S_y = \frac{R_y - I_y}{R_z - I_z}. \quad (2)$$

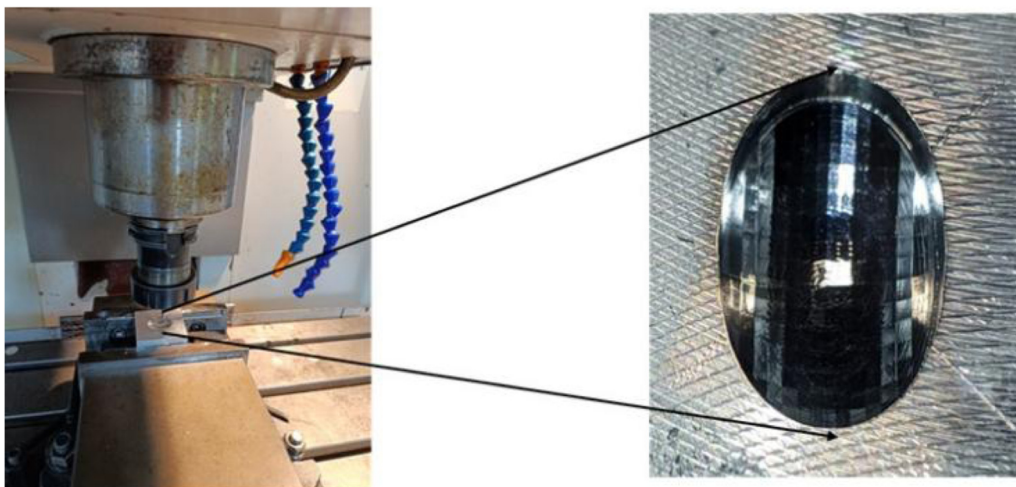


FIGURE 8
Mold machining process.

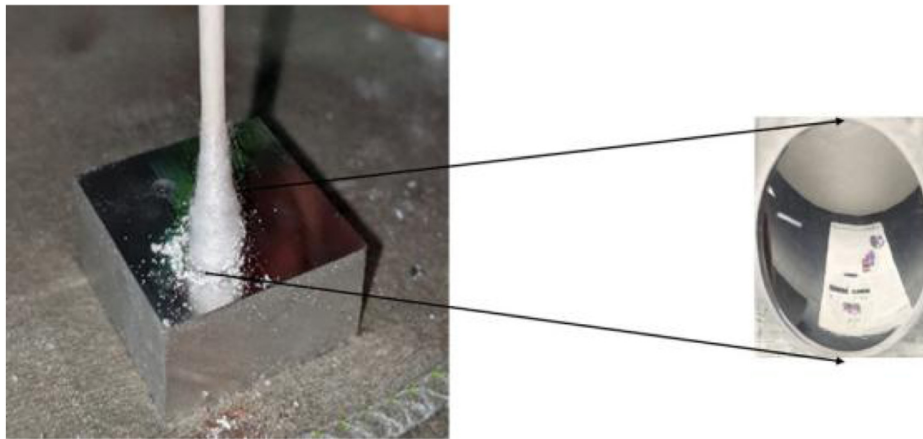


FIGURE 9
Manual polishing using a cotton swab to erase machining traces.

The shape of the surface can be obtained using the following line integral Equation 3:

$$z = z_0 + \int (S_x dx + S_y dy), \quad (3)$$

where z_0 is the z coordinate of the design surface vertex. The trapezoidal rule was implemented to recover the point cloud (x, y, z) describing the surface under test (Huerta-Carranza et al., 2021; Huerta-Carranza et al., 2025).

On the other hand, a second surface evaluation was performed using the coordinate measurement technique, using a stylus (Edmund Optics Spherometer Kit) and a two-axis micrometric displacement system (Bosch, 2012; Zhang et al., 1985; Shen et al., 2023; Michihata, 2022). The implemented arrangement is shown in Figure 7.

Height measurements were made along the major axis (YZ plane) and minor axis (XZ plane) to find the values of the radii of curvature along these directions. The process involves measuring the coordinates at various points on the surface, fitting a polynomial function to the measured points, and determining the radii of curvature in both directions.

5 Results, analysis, and discussions

After applying a stage of manual polishing (Figures 8, 9), images of the mold surface were captured using an Olympus BX 51 optical microscope, with a pixel size of $0.15 \mu\text{m}$, and using the Fiji program (Schindelin et al., 2012), the surface roughness was measured by taking a line, yielding a roughness $R_q = 165.5$; Figure 10 shows the roughness profile.

Once the mold was polished, its finish quality was verified using optical tests. First, the null screen test was implemented; a photograph of the experimental arrangement setup, together with the image obtained, is shown in Figure 11.

Figure 12a shows the desired ideal image used to design the object pattern, and Figure 12b shows the experimental image obtained.

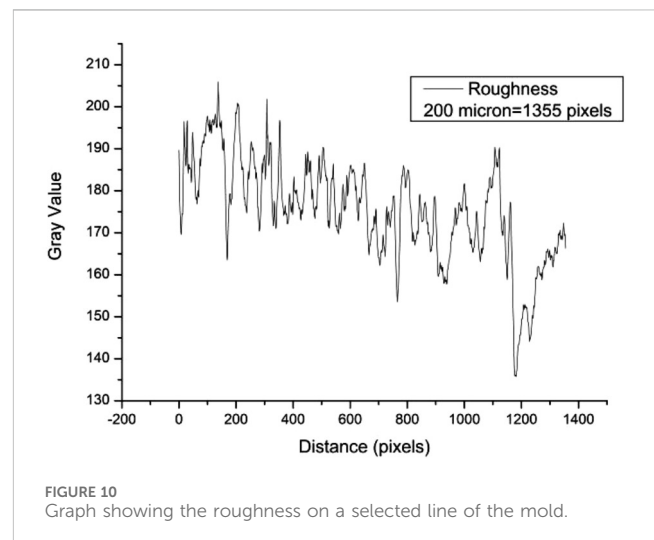


FIGURE 10
Graph showing the roughness on a selected line of the mold.

When processing the obtained image, quantitative results are obtained and shown in Table 2. The coefficients found are used to calculate the radii of curvature of the toroidal surface.

The terms A_0 , A_1 , and A_2 do not deform the surface and can be ignored; therefore, the polynomial representing the surface is presented in Equation 4:

$$z = 0.020 x^2 - 0.0005 xy + 0.008 y^2. \quad (4)$$

A 3D graph of the reconstructed surface is shown in Figure 13a, and a contour map of the reconstructed mold face is presented in Figure 13b. Finally, Figure 14 shows the map of differences between the ideal surface and the generated surface, yielding a PV of 0.1806 mm and an RMS of 0.0402 mm . In these tests, the error was obtained when comparing the point cloud with the points of the ideal surface rather than with the best-fit surface; hence, the peak–valley error is larger.

Since the arrangement is expected to be a horizontal and vertical distribution of spots, the image (Figure 12b) shows slight deviations in the horizontal spots and that the pictures appear

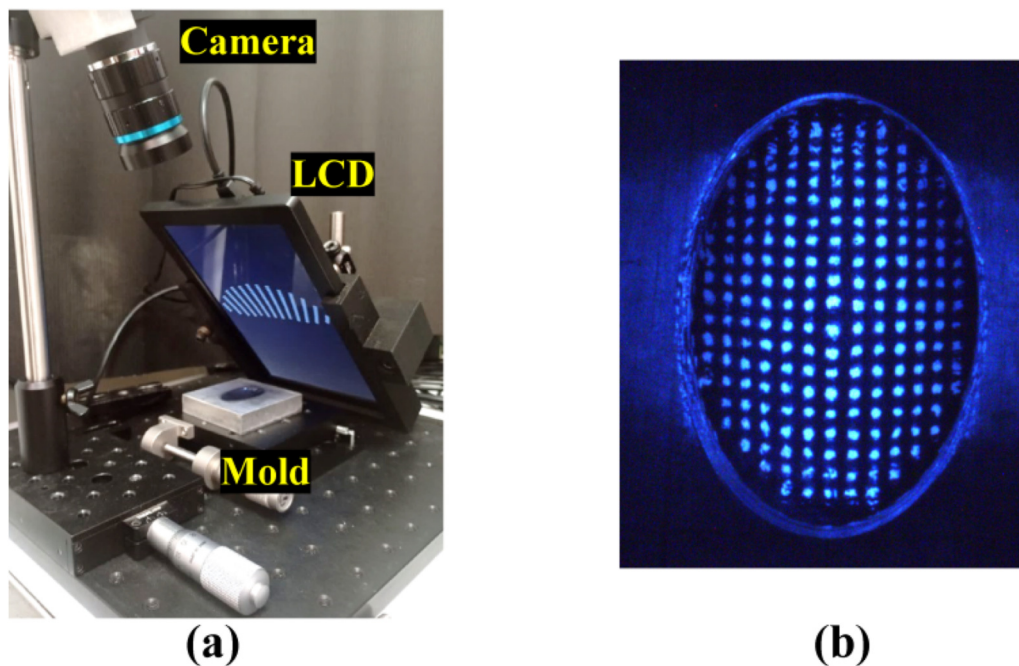


FIGURE 11 (a) Experimental null screen test arrangement implemented; (b) image obtained.

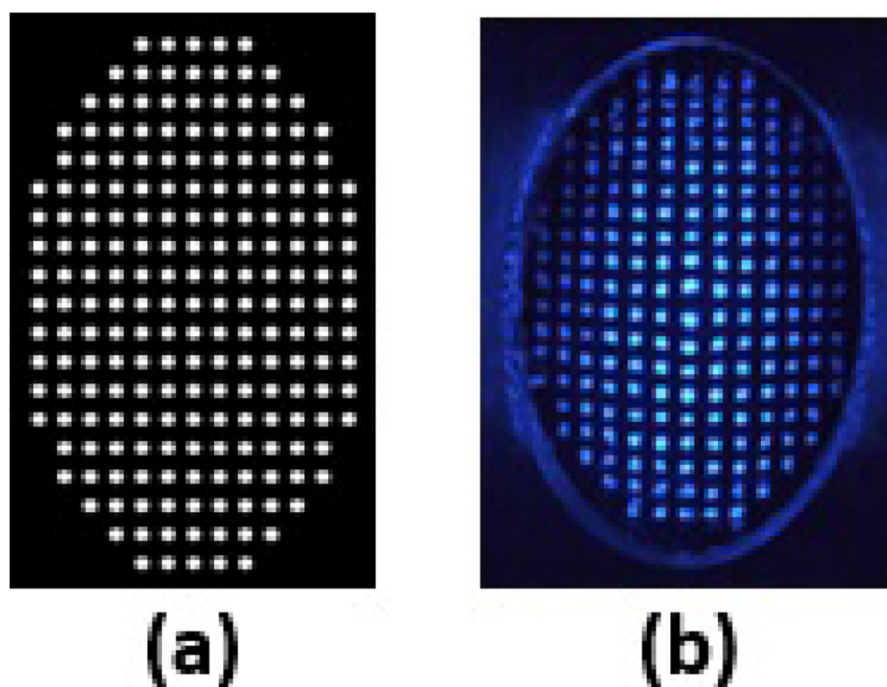


FIGURE 12 (a) Ideal image; (b) experimental image.

smaller at the top than at the bottom, which translates into slight variations of the radii of curvature in both directions. We assume that these variations are small as large deviations would result in

more pronounced defects in the obtained image. On the other hand, when examining the map of differences between surfaces, we observe that the surface exhibits greater deviations along the

TABLE 2 Geometrical parameters obtained for the toroidal mold.

Coefficient polynomial	Radii of curvature
$A_0 = -2.047$	$R_x = 24.54$ mm
$A_1 = -0.007$	
$A_2 = 0.035$	$R_y = 60.47$ mm
$A_3 = 0.020$	
$A_4 = -0.0005$	
$A_5 = 0.008$	

edges in the horizontal direction. The center of the surface is where the best fit between the surfaces occurs. Therefore, it can be concluded that the proposed methodology using a traditional machining center is feasible for manufacturing molds without rotational symmetry.

Likewise, when applying the coordinate measurement test, a database was generated; coordinates of the points found are shown in the graphs in Figure 15. A quadratic adjustment was applied to the distributions of the detected points, where the polynomials used to perform the fit in the x- and y-directions are given by Equations 5, 6:

$$z = B_0 + B_1(y - y_0) + B_2(y - y_0)^2, \quad (5)$$

and

$$z = D_0 + D_1(x - x_0) + D_2(x - x_0)^2. \quad (6)$$

The values of the coefficients found are provided in Table 3, with which the radii of curvature are calculated, given by $R_x = 1/(2 B_2)$ and $R_y = 1/(2 D_2)$.

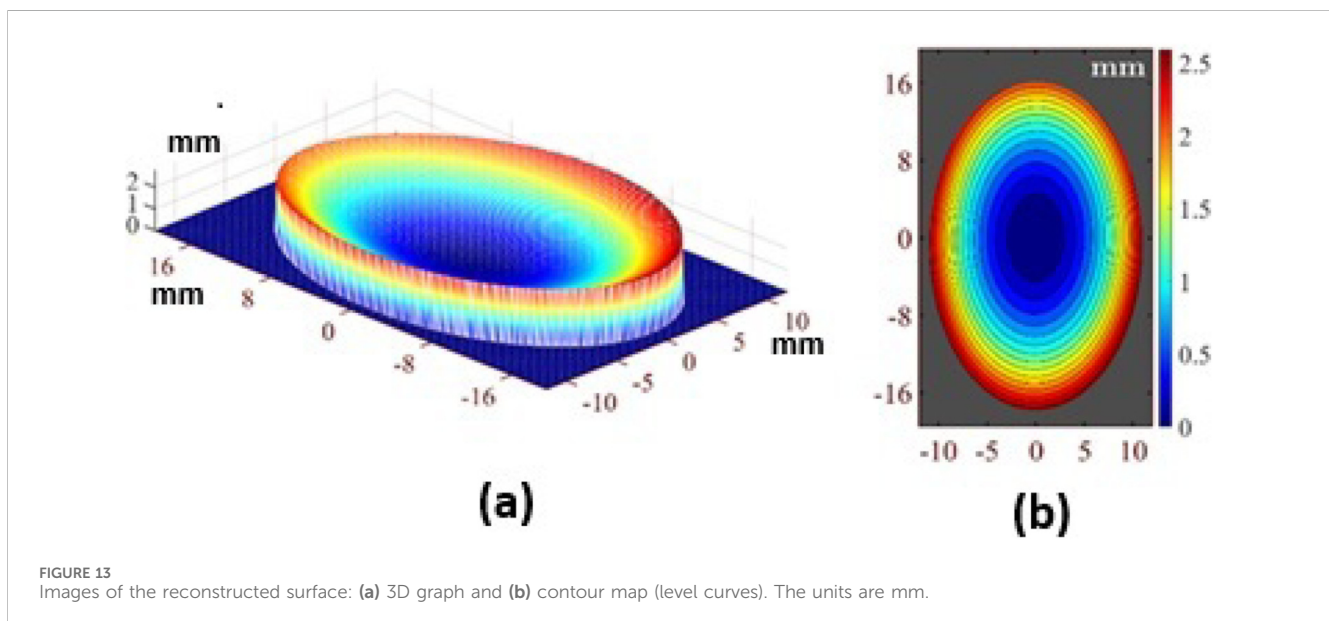
Figure 16 shows a map of differences between the ideal surface and the surface found, yielding a PV of 0.2366 mm and an RMS of 0.0506 mm.

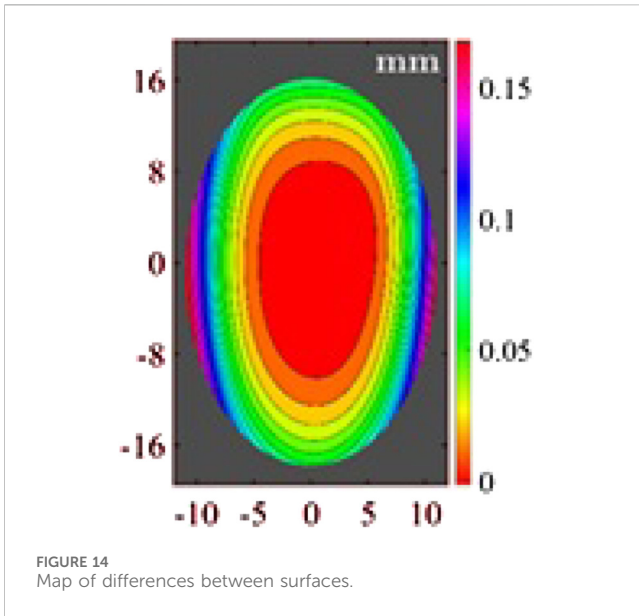
When analyzing the map of differences between the ideal surface and the reconstructed surface, it is observed that there are slight variations in the poles of the curves, and in the central part, there are slight variations in the symmetry that would be expected in the curves, as shown in Figure 16. On the other hand, when the polynomial fits were made in the x- and y-directions, the surfaces exhibit minimal deviations, as indicated by the PV and RMS values, which are of the same order as those obtained using the null screen technique.

The implemented test methods are effective for evaluating convex surfaces with $f/\# < 1$ and freeform surfaces at low cost, whereas other tests require complementary elements, such as holograms or reference surfaces, which increase their cost. Since the radii of curvature in the x- and y-directions vary by nearly a factor of three, for some tests, it is not possible to evaluate the entire surface area in a single measurement. The null screen test does not present this difficulty and allows measuring the surface profile by quantifying the deviations computationally, but it depends on the resolution of the CCD camera and the display used in the test. On the other hand, the measurement of coordinates does not present such problems, and its resolution depends on the arrangement implemented, the precision of the mounts used to make the displacement, and the resolution of the probe (stylus). Quantification is carried out computationally by integrating the information and knowing the shape of the surface. The disadvantage of the latter technique is that it can scratch the surface.

In future work, these tests will be implemented to guide the polishing stage, enabling a better match with the expected values in the surface design.

According to the measurements, the null screen test yields better results than coordinate measurement. Despite the emergence of recent freeform mold-manufacturing techniques, CNC milling is still an alternative due to its accessibility and low cost, but it is necessary to strengthen the finishing process, implementing a polishing stage along with optical tests to guide this process.





The use of manufacturing simulations allowed the validation of machining operations and the determination of ranges for selecting the manufacturing parameters to be applied.

The manual polishing process allows the elimination of machining traces; however, its localized nature introduces deviations in the surface profile and roughness, which will

need to be analyzed to determine how to minimize its effect. On the other hand, when applying the optical tests to determine the shape of the surface, it was found that both tests obtain deviations of the same order, but the combination of the radii of curvature found with the measurement of coordinates is better suited to the ideal values of the surface of the mold, although the null screen test obtains lower PV and RMS deviations.

Therefore, the proposed methodology for manufacturing aluminum molds uses conventional instruments, which reduces the cost of production compared to modern techniques (considering the high number of components that can be manufactured with the mold). Finally, because the surface lacks rotary symmetry, its contour is not circular, and the radii of curvature in the x- and y-directions differ significantly, which makes manufacturing and testing difficult, as only a limited number of low-cost tests can be applied.

6 Conclusion

A comprehensive methodology to elaborate freeform molds using a five-axis machining center was presented. It is shown that the generation of this type of mold in aluminum with the desired shape is possible as a low-cost alternative to existent technologies. The manufacture of the part begins with the optical design, validating its optical performance and the use of valid

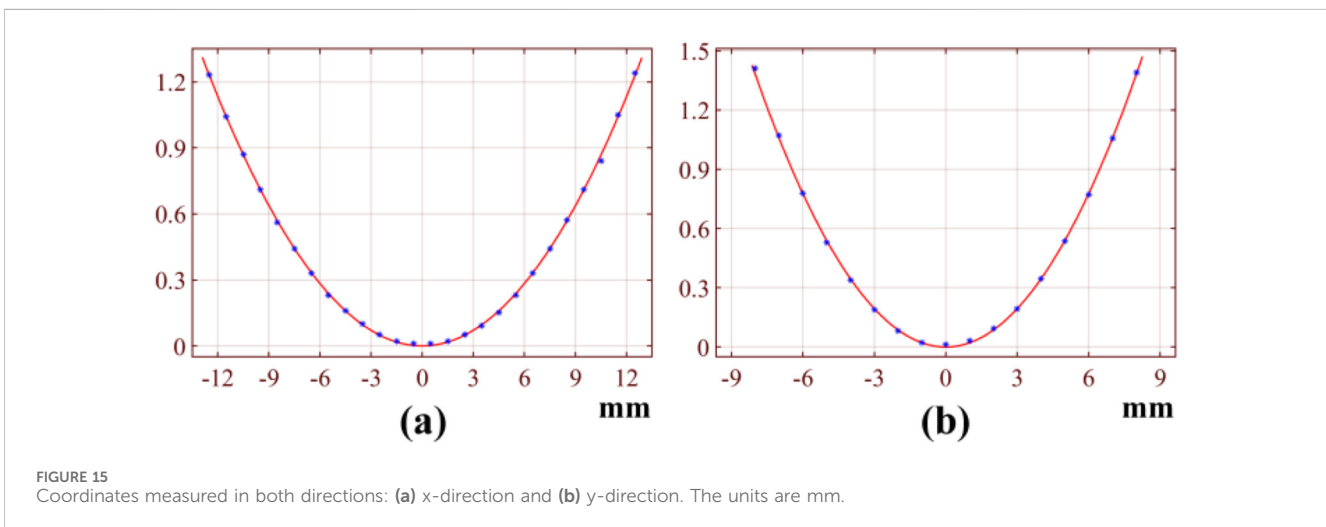
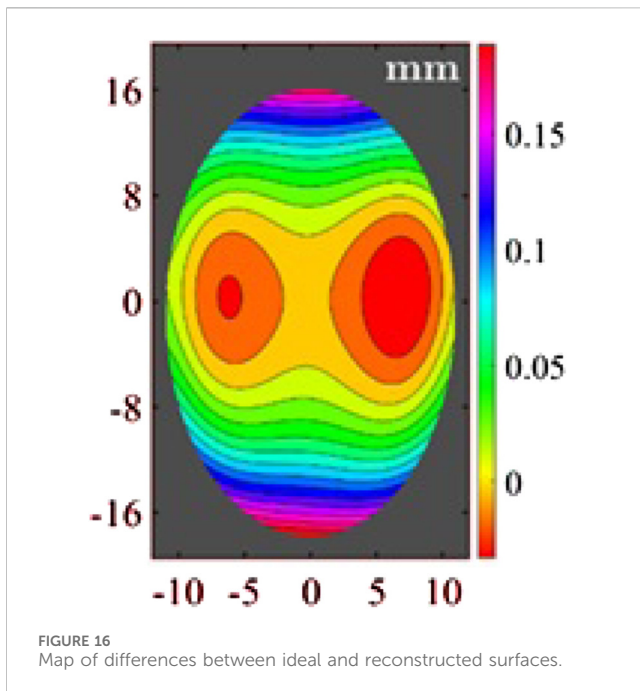


TABLE 3 Coefficients and radii of curvature found.

Parameters in the y-direction	Parameters in the x-direction
$B_0 = -0.00014$	$D_0 = 0.000042$
$B_1 = -0.00007$	$D_1 = 0.000032$
$B_2 = 0.00785$	$D_2 = 0.021602$
$Y_0 = 11.01253$	$X_0 = 11.000036$
$Ry = 63.7124 \text{ mm}$	$Rx = 23.1457 \text{ mm}$



machining processes for the milling machine through simulations. Likewise, it is shown that a polishing stage is required to improve and guide the finishing of the manufactured mold and reduce the tool marks left by the cutters.

Finally, the null screen and coordinate measurement tests allowed the quality of the machined surface to be evaluated, qualitatively demonstrating that the deviations of the desired profile are minimal; these tests were simple and straightforward to implement and evaluate, considering that the shape of the generated surface has no symmetry of revolution. The surface contour is not circular, and there is a difference in the radii of curvature of the X- and Y-axes. The results obtained are encouraging, but a design of experiments is required to find the best combination of machining parameters to produce a surface with minimal roughness. A polishing stage is necessary to improve the surface finish, requiring further studies to achieve greater precision. Although the tests applied to assess the mold surface demonstrate similar accuracy, it is necessary to explore variations of the null screen to improve evaluation precision and investigate other applicable tests that can further improve accuracy.

Data availability statement

The raw data supporting the conclusions of this article will be made available by the authors, without undue reservation.

References

Aguirre-Aguirre, D., Campos-García, M., Díaz-Uribe, R., and Villalobos-Mendoza, B. (2018). General equations for the null-screen test for aspherical surfaces with deformation coefficients. *Appl. Opt.* 57 (35), 10230. doi:10.1364/AO.57.010230

Author contributions

AS-A: Conceptualization, Formal analysis, Investigation, Methodology, Writing – original draft, Writing – review and editing. FG-A: Conceptualization, Investigation, Resources, Supervision, Validation, Writing – review and editing. OH-C: Conceptualization, Data curation, Formal analysis, Investigation, Methodology, Resources, Validation, Visualization, Writing – review and editing. VC-M: Conceptualization, Formal analysis, Methodology, Software, Visualization, Writing – review and editing. JA-M: Methodology, Software, Validation, Visualization, Writing – review and editing. MA-A: Investigation, Resources, Supervision, Validation, Visualization, Writing – review and editing.

Funding

The author(s) declared that financial support was received for this work and/or its publication. The authors acknowledge the economic support received by CONAHCYT for the sabbatical fellowship to Agustin Santiago Alvarado (CVU 710606) by number project I0200/111/2024.

Conflict of interest

The author(s) declared that this work was conducted in the absence of any commercial or financial relationships that could be construed as a potential conflict of interest.

Generative AI statement

The author(s) declared that generative AI was not used in the creation of this manuscript.

Any alternative text (alt text) provided alongside figures in this article has been generated by Frontiers with the support of artificial intelligence, and reasonable efforts have been made to ensure accuracy, including review by the authors wherever possible. If you identify any issues, please contact us.

Publisher's note

All claims expressed in this article are solely those of the authors and do not necessarily represent those of their affiliated organizations, or those of the publisher, the editors and the reviewers. Any product that may be evaluated in this article, or claim that may be made by its manufacturer, is not guaranteed or endorsed by the publisher.

- Atwood, C., Griffith, M., Harwell, L., Schlienger, E., Ensz, M., Smugeresky, J., et al. (1998). "Laser engineered net shaping (LENSTM): a tool for direct fabrication of metal parts," in *En: international congress on applications of lasers and electro-optics*. Orlando, Florida, USA: Laser Institute of America.
- Avendaño-Alejo, M., Moreno-Oliva, V. I., Campos-García, M., and Díaz-Urbe, R. (2009). Quantitative evaluation of an off-axis parabolic mirror by using a tilted null screen. *Appl. Opt.* 48 (5), 1008. doi:10.1364/AO.48.001008
- Bohórquez, C. A., Sierra Cetina, M., and Lemus, J. (2010). Influencia del tratamiento térmico de envejecimiento en las propiedades mecánicas de los aluminios 6061 T6 y 6063 T5. *Av Investig En Ing.* 13(1):20.
- Bosch, J. A. (2012). *Coordinate measuring machines and systems*. 2nd ed (Boca Raton, FL: CRC/Taylor and Francis), 1.
- Brenner, K. H., Kufner, M., Kufner, S., Moisel, J., Müller, A., Sinzinger, S., et al. (1993). Application of three-dimensional micro-optical components formed by lithography, electroforming, and plastic molding. *Appl. Opt.* 32 (32), 6464–6469. doi:10.1364/AO.32.006464
- Broemel, A., Lippmann, U., and Gross, H. (2017). Freeform surface descriptions. Part I: mathematical representations. *Adv. Opt. Technol.* 6 (5), 327–336. doi:10.1515/aot-2017-0030
- Carrasco Morcillo, R. (2019). *Evolución histórica de los materiales usados para las lentes de contacto*. Valladolid: Bucle consorcio. Available online at: <http://uvadoc.uva.es/handle/10324/38376> (Accessed July 29, 2025).
- Chen, J. J., Wang, T. Y., Huang, K. L., Liu, T. S., Tsai, M. D., and Lin, C. T. (2012). Freeform lens design for LED collimating illumination. *Opt. Express*. 20 (10), 10984–10995. doi:10.1364/OE.20.10984
- Chen, L., Kirchberg, S., Jiang, B. Y., Xie, L., Jia, Y. L., and Sun, L. L. (2014). Fabrication of long-focal-length plano-convex microlens array by combining the micro-milling and injection molding processes. *Appl. Opt.* 53 (31), 7369–7380. doi:10.1364/AO.53.007369
- Coppermetal (2025). Coppermetal Disponible en. Available online at: <https://www.coppermetal.com.br/es/blog/aluminio-6061/#:~:text=El%20aluminio%206061%20es%20una,%20soldabilidad%20C%20y%20mucho%20m%C3%A1s> (Accessed October 14, 2025).
- Davis, G. E., Roblee, J. W., and Hedges, A. R. (2009). "Comparison of freeform manufacturing techniques in the production of monolithic lens arrays. En: burge JH, fähle OW, williamson R, editores," San Diego, CA. Available online at: <http://proceedings.spiedigitallibrary.org/proceeding.aspx?doi=10.1117/12.824451> (Accessed September 23, 2025).
- Díaz-Urbe, R., and Campos-García, M. (2000). Null-screen testing of fast convex aspheric surfaces. *Appl. Opt.* 39 (16), 2670. doi:10.1364/AO.39.002670
- Ding, Y., Liu, X., Zheng, Z. rong, and Gu, P. fu (2008). Freeform LED lens for uniform illumination. *Opt. Express*. 16 (17), 12958–12966. doi:10.1364/oe.16.012958
- Elgarisi, M., Frumkin, V., Luria, O., and Bercovici, M. (2021). Fabrication of freeform optical components by fluidic shaping. *Optica*. 8 (11), 1501. doi:10.1364/optica.438763
- Fang, F. Z., Zhang, X. D., Weckenmann, A., Zhang, G. X., and Evans, C. (2013a). Manufacturing and measurement of freeform optics. *CIRP Ann.* 62 (2), 823–846. doi:10.1016/j.cirp.2013.05.003
- Fang, F., Cheng, Y., and Zhang, X. (2013b). Design of freeform optics. *aot*. 2 (5-6), 445–453. doi:10.1515/aot-2013-0029
- Gates, B. D., Xu, Q., Stewart, M., Ryan, D., Willson, C. G., and Whitesides, G. M. (2005). New approaches to nanofabrication: molding, printing, and other techniques. *Chem. Rev.* 105 (4), 1171–1196. doi:10.1021/cr030076o
- Gross, H., Brömel, A., Beier, M., Steinkopf, R., Hartung, J., Zhong, Y., et al. (2015). "Overview on surface representations for freeform surfaces," Jena, Germany. Available online at: <http://proceedings.spiedigitallibrary.org/proceeding.aspx?doi=10.1117/12.2191255> (Accessed July 04, 2025).
- Gurganus, D., Novak, S., Symmons, A., and Davies, M. A. (2019). *Precision glass molding of freeform optics. En: optical design and fabrication 2019 (freeform, OFT)*. Washington, DC: OSA.
- Hazir, E., Erdinler, E. S., and Koc, K. H. (2018). Optimization of CNC cutting parameters using design of experiment (DOE) and desirability function. *J For Res.* 29 (5), 1423–1434. doi:10.1007/s11676-017-0555-8
- He, R., Teng, C., Kumar, S., Marques, C., and Min, R. (2022). Polymer optical fiber liquid level sensor: a review. *IEEE Sens* 15 enero22 (2), 1081–1091. doi:10.1109/jsen.2021.3132098
- Huang, C. (2008). *Investigation of injection molding process for high precision polymer lens manufacturing*. Ohio State University.
- Huerta-Carranza, O., Avendaño-Alejo, M., and Díaz-Urbe, R. (2021). Null screens to evaluate the shape of freeform surfaces: progressive addition lenses. *Opt. Express* 29 (17), 27921–27937. doi:10.1364/OE.434289
- Huerta-Carranza, O., Granados-Agustín, F. S., Santiago-Alvarado, A., Campos-García, M., and Avendaño-Alejo, M. (2024). Evaluation of the aspherical surface of a plano-convex lens by refraction using an LCD. *Rev Sci Instrum.* 95 (9), 095113. doi:10.1063/5.0198152
- Huerta-Carranza, O., Granados-Agustín, F., Campos-García, M., Santiago-Alvarado, A., and Avendaño-Alejo, M. (2025). Improvement in the implementation of a null test to evaluate a parabolic trough solar collector using an off-axis configuration. *J. Renew. Sustain Energy* 17 (2), 023701. doi:10.1063/5.0252276
- Kumar, S., Tong, Z., and Jiang, X. (2022). Advances in the design and manufacturing of novel freeform optics. *Int. Extreme Manuf.* 4 (3), 032004. doi:10.1088/2631-7990/ac7617
- Lasemi, A., Xue, D., and Gu, P. (2010). Recent development in CNC machining of freeform surfaces: a state-of-the-art review. *Comput-Aided* 42 (7), 641–654. doi:10.1016/j.cad.2010.04.002
- Lee, B. G., and Scherer, A. (2001). "Diffractive lens fabrication by replica molding. En," in *Technical digest summaries of papers presented at the conference on lasers and electro-optics postconference technical digest (IEEE cat No01CH37170)*. Baltimore, MD, USA: IEEE.
- Li, H., Li, L., Naples, N. J., Roblee, J. W., and Yi, A. Y. (2017). Micro-optical fabrication by ultraprecision diamond machining and precision molding. *Front. Mech. Eng.* 12 (2), 181–192. doi:10.1007/s11465-017-0444-z
- Li, K., Xu, G., Huang, X., Xie, Z., and Gong, F. (2018). Manufacturing of micro-lens array using contactless micro-embossing with an EDM-mold. *Appl. Sci.* 9 (1), 85. doi:10.3390/app9010085
- Li, Y., Li, K., and Gong, F. (2021). Fabrication and optical characterization of polymeric aspherical microlens array using hot embossing technology. *Appl. Sci.* 11 (2), 882. doi:10.3390/app11020882
- Liu, X., Zhang, L., Zhou, W., Zhou, T., Yu, J., Lee, L. J., et al. (2019). Fabrication of plano-concave plastic lens by novel injection molding using carbide-bonded graphene-coated silica molds. *Manuf. Sci. Eng.* 141 (8), 081011. doi:10.1115/1.4043980
- Loadi, D., Quagliotti, D., Calaan, M., Parenti, P., Annoni, M., and Tosello, G. (2018). Manufacturing signatures of injection molding and injection compression molding for micro-structured polymer fresnel lens production. *Micromachines.* 10 diciembre9 (12), 653. doi:10.3390/mi9120653
- Lu, X., and Khim, L. S. (2001). A statistical experimental study of the injection molding of optical lenses. *Mater. Process Technol.* 113 (1-3), 189–195. doi:10.1016/s0924-0136(01)00606-9
- Mali, R. A., Gupta, T. V. K., and Ramkumar, J. (2021). A comprehensive review of free-form surface Milling— advances over a decade. *J. Manuf. Process* 62, 132–167. doi:10.1016/j.jmapro.2020.12.014
- Mayer, R. (2007). Precision injection molding: how to make polymer optics for high volume and high precision applications. *Opt. Photonik.* 2 (4), 46–51. doi:10.1002/opph.201190286
- Michaeli, W., Hessner, S., and Klaiber, F. (2009). Analysis of different compression-molding techniques regarding the quality of optical lenses. *Vac Sci Technol B Microelectron Nanom. Struct. Process Meas. Phenom.* 27 (3), 1442–1444. doi:10.1116/1.3079765
- Michihata, M. (2022). Surface-sensing principle of microprobe system for micro-scale coordinate metrology: a review. *Metrol.* 2 (1), 46–72. doi:10.3390/metrology2010004
- Moon, S. Dong, Lee, N., and Kang, S. (2003). Fabrication of a microlens array using micro-compression molding with an electroformed mold insert. *Micromechanics Microengineering.* 13 (1), 98–103. doi:10.1088/0960-1317/13/1/314
- Moskaleva, A., Safonov, A., and Hernández-Montes, E. (2021). Fiber-reinforced polymers in freeform structures: a review. *Buildings.* 16 Oct.11 (10), 481. doi:10.3390/buildings11100481
- Ottevaere, H., Volckaerts, B., Vervaeke, M., Vynck, P., Hermanne, A., and Thienpont, H. (2004). Plastic microlens arrays by deep lithography with protons: fabrication and characterization. *Jpn. J. Appl. Phys.* 43 (8S), 5832. doi:10.1143/jjap.43.5832
- Ottevaere, H., Cox, R., Herzig, H. P., Miyashita, T., Naessens, K., Taghizadeh, M., et al. (2006). Comparing glass and plastic refractive microlenses fabricated with different technologies. *Opt Pure Appl. Opt.* 8 (7), S407–S429. doi:10.1088/1464-4258/8/7/s18
- Peixoto, C., Valentim, P. T., Sousa, P. C., Dias, D., Araújo, C., Pereira, D., et al. (2022). Injection molding of high-precision optical lenses: a review. *Precis. Eng.* 76, 29–51. doi:10.1016/j.precisioneng.2022.02.002
- Pelin, G., Sonmez, M., and Pelin, C. E. (2024). The use of additive manufacturing techniques in the development of polymeric molds: a review. *Polym.* 16 (8), 1055. doi:10.3390/polym16081055
- Roeder, M., Guenther, T., and Zimmermann, A. (2019). Review on fabrication technologies for optical mold inserts. *Micromachines.* 3 10 (4), 233. doi:10.3390/mi10040233
- Rolland, J. P., Davies, M. A., Suleski, T. J., Evans, C., Bauer, A., Lambropoulos, J. C., et al. (2021). Freeform optics for imaging. *Opt.* 8 (2), 161. doi:10.1364/optica.413762
- Santiago-Alvarado, A., Granados-Agustín, F. S., Percino-Zacarias, M. E., Huerta-Carranza, O., and Moreno Oliva, V. I. (2023). "Evaluation of aluminum molds using the null screens test. En: barnes BM," in *Editores. Modeling aspects in optical metrology IX*. Munich, Germany: SPIE.
- Santiago-Alvarado, A., Granados-Agustín, F. S., Percino-Zacarias, M. E., Cruz-Martínez, V. M., Huerta-Carranza, O., Alvarado-Martínez, J. D. J., et al. (2025).

- “Methodology to manufacturing and testing freeform aluminum mold,” in *Optical measurement systems for industrial inspection XIV*. Munich, Germany: SPIE.
- Schindelin, J., Arganda-Carreras, I., Frise, E., Kaynig, V., Longair, M., Pietzsch, T., et al. (2012). Fiji: an open-source platform for biological-image analysis. *Nat. Methods*. 9 (7), 676–682. doi:10.1038/nmeth.2019
- Sha, W., Xiao, M., Zhang, J., Ren, X., Zhu, Z., Zhang, Y., et al. (2021). Robustly printable freeform thermal metamaterials. *Nat. Commun.* 12 (1), 7228. doi:10.1038/s41467-021-27543-7
- Shen, Y., Ren, J., Huang, N., Zhang, Y., Zhang, X., and Zhu, L. (2023). Surface form inspection with contact coordinate measurement: a review. *Int. Extreme Manuf.* 5 (2), 022006. doi:10.1088/2631-7990/acc76e
- Singh, I. A. S. G. K., Reddy, T. N., and Vinod, P. (2021). Freeform machining of ophthalmic toric lens mould using fast tool servo-assisted ultra-precision diamond turning process. *Micromanufacturing*. 4 (1), 84–92. doi:10.1177/2516598420939745
- Spina, R., Walach, P., Schild, J., and Hopmann, C. (2012). Analysis of lens manufacturing with injection molding. *Int. Precis. Eng. Manuf.* 13 (11), 2087–2095. doi:10.1007/s12541-012-0276-z
- Visconti, A. J., Fang, K., Corsetti, J. A., McCarthy, P., Schmidt, G. R., and Moore, D. T. (2013). Design and fabrication of a polymer gradient-index optical element for a high-performance eyepiece. *Opt. Eng.* 52 (11), 112107. doi:10.1117/1.oe.52.11.112107
- Ye, J., Chen, L., Li, X., Yuan, Q., and Gao, Z. (2017). Review of optical freeform surface representation technique and its application. *Opt. Eng.* 56 (11), 1. doi:10.1117/1.oe.56.11.110901
- Yu, H., Zhou, G., Chau, F. S., and Lee, F. (2009). Fabrication and characterization of PDMS microlenses based on elastomeric molding technology. *Opt. Lett.* 34 (21), 3454–3456. doi:10.1364/OL.34.003454
- Zhan, Z., Wang, K., Yao, H., and Cao, Z. (2009). Fabrication and characterization of aspherical lens manipulated by electrostatic field. *Appl. Opt.* 48 (22), 4375–4380. doi:10.1364/ao.48.004375
- Zhang, L., and Liu, W. (2017). Precision glass molding: toward an optimal fabrication of optical lenses. *Front. Mech. Eng.* 12 (1), 3–17. doi:10.1007/s11465-017-0408-3
- Zhang, G., Veale, R., Charlton, T., Borchardt, B., and Hocken, R. (1985). Error compensation of coordinate measuring machines. *CIRP Ann.* 34 (1), 445–448. doi:10.1016/s0007-8506(07)61808-3
- Zhong, Z. W. (2020). Advanced polishing, grinding and finishing processes for various manufacturing applications: a review. *Mater Manuf Process.* 35 (12), 1279–1303. doi:10.1080/10426914.2020.1772481
- Zhou, T., He, Y., Wang, T., Zhu, Z., Xu, R., Yu, Q., et al. (2021). A review of the techniques for the mold manufacturing of micro/nanostructures for precision glass molding. *Int. Extreme Manuf.* 3 (4), 042002. doi:10.1088/2631-7990/ac1159